



Short communication

Carbon supported Pd–Ni–P nanoalloy as an efficient catalyst for ethanol electro-oxidation in alkaline media



Ye Wang ^a, Fei-Fei Shi ^b, Yao-Yue Yang ^a, Wen-Bin Cai ^{a,*}

^a Shanghai Key Laboratory for Molecular Catalysis and Innovative Materials, Collaborative Innovation Center of Chemistry for Energy Materials and Department of Chemistry, Fudan University, Shanghai 200433, China

^b Department of Mechanical Engineering, University of California, Berkeley, CA 94720, USA

HIGHLIGHTS

- Initial synthesis of Pd–Ni–P/C ternary nanocatalyst for ethanol electro-oxidation in alkaline media.
- Significantly enhanced electrocatalytic performance on Pd–Ni–P/C compared to that on Pd/C, Pd–P/C or Pd–Ni/C.
- Electronic, geometric and bifunctional effects assumed to account for the improved performance.

ARTICLE INFO

Article history:

Received 4 February 2013

Received in revised form

4 June 2013

Accepted 4 June 2013

Available online 13 June 2013

Keywords:

Carbon supported palladium–nickel–phosphorus

Electrocatalyst

Ethanol oxidation reaction (EOR)

Alkaline media

ABSTRACT

Carbon-supported well-dispersed Pd–Ni–P ternary catalyst targeted for ethanol oxidation reaction (EOR) in alkaline media is synthesized in a simple aqueous bath containing Pd(II) and Ni(II) salts with sodium hypophosphite as the reducing agent and the source for P and sodium citrate as the complexing agent. XRD analysis on the as-prepared Pd–Ni–P/C reveals that Ni shrinks while P expands the Pd lattice structure, and XPS measurement suggests different electronic effects of the two alloying elements on Pd. Cyclic voltammetry and chronoamperometry indicate that the Pd–Ni–P/C presents a remarkably higher electrocatalytic activity than the state-of-the-art Pd/C, Pd–P/C and Pd–Ni/C catalysts. This may be ascribed to the unique electronic, geometric and bifunctional effects involved in this ternary nanoalloy.

© 2013 Elsevier B.V. All rights reserved.

1. Introduction

Nowadays, direct ethanol fuel cells have predominantly relied on Pt-based anode catalysts in acidic media [1]. Nevertheless, there is a surge of interest in developing alkaline polymer electrolyte fuel cells largely because facile ethanol oxidation reaction (EOR) kinetics may occur at less costly and more abundant Pd-based catalysts in basic media rather than in acidic media [2,3]. In general, two distinct pathways are proposed for EOR: One goes via CO_{ads} intermediate followed by further oxidation with reactant pair OH_{ads} or O_{ads} to form CO_2 and the other involves no cleavage of C–C bond via acetaldehyde to form acetic acid [3,4]. Accordingly, efficient electrocatalysts could be designed through the manipulation of their composition and structure by taking advantages of electronic,

geometric and/or bifunctional effects [5]. Along this line, many Pd-based bimetallic catalysts including but not limited to Pd–Ni/C [6], Pd–Ru/C [7] and Pd/oxide/C [8] and trimetallic catalysts such as Pd–Ni–Au/C [9] have been reported, in particular, Pd–Ni/C seems to be the most cost-effective catalyst for EOR in alkaline media.

On the other hand, metal–nonmetal alloy catalysts are under development, with an expectation that the nonmetal component may also promote the electrocatalytic activity of the primary metal by modifying its electronic and geometric properties [10,11]. In fact, Pd–B/C [12] or Pd–P/C [13] turns out to be more active than Pd/C in electro-oxidizing formic acid, and Pt–Sn–P/C [14] is more active than Pt–Sn/C in electro-oxidizing ethanol in acidic media.

In the pursuit of more efficient Pd-based catalysts for EOR, ternary nanoalloys incorporating suitable assistive metal and metalloid components are expected to exhibit more flexibility in tuning the geometric and electronic properties of Pd surfaces, thus are promising to achieve a higher electrocatalytic performance [5]. Nevertheless, such ternary catalysts have not been reported to our

* Corresponding author. Tel.: +86 21 55664050; fax: +86 21 65641740.

E-mail address: wbcai@fudan.edu.cn (W.-B. Cai).

best knowledge. In this preliminary work, we synthesize for the first time a Pd–Ni–P/C catalyst through a facile wet chemical process. The new catalyst is characterized by different analytical tools, tested for EOR in alkaline media and compared with the state-of-the-art Pd/C, Pd–P/C and Pd–Ni/C catalysts.

2. Experimental

2.1. Preparation of catalysts

The ternary catalyst was prepared through an aqueous solution phase synthesis. Specifically, 0.22 g of sodium citrate, 0.039 g of NiSO_4 and 3 mL of 0.05 M PdCl_2 (containing 0.27 M NaCl) were mixed into a 10 mL solution. The pH value was adjusted to 10, and then 60 mg of Vulcan XC-72 carbon black was added. After the solution was sonicated for 30 min, 10 mL of 0.1 M NaH_2PO_2 was added dropwisely to the slurry through a peristaltic pump at the rate of 0.5 mL min^{-1} under vigorous stirring. After being continuously stirred at 80 °C for 4 h, the resulted suspension was filtered, washed with ultrapure Milli-Q water ($>18 \text{ M}\Omega\cdot\text{cm}$) and vacuum-dried at 70 °C for 6 h.

The Pd–P/C catalyst was also prepared in the same procedure except that Ni(II) was absent, largely based on the work reported by Lu's group [13], leading to $\text{Pd}_{11}\text{P}_1/\text{C}$. The $\text{Pd}_2\text{Ni}_3/\text{C}$ catalyst was selectively prepared by simultaneous reduction process with NaBH_4 as the reductant according to Reference 6, since the $\text{Pd}_2\text{Ni}_3/\text{C}$ showed the best performance for EOR in alkaline media among the Pd–Ni/C bimetallic catalysts reported therein. 20 wt.% Pd was set for all the home-made samples. A state-of-the-art commercial Pd/C catalyst (40 wt.%, BASF) served as the reference sample.

2.2. Characterization of catalysts

The structural and compositional properties of the Pd-based nanoparticles were characterized on a JEOL JEM-2010 microscope for TEM, on a Hitachi P-4010 for ICP-AES, on a D8 Advance X-ray Diffractometer with $\text{Cu K}\alpha$ radiation from 30 to 90° for XRD and on a Kratos Axis Ultra^{DLD} with an $\text{Al K}\alpha$ X-ray (1486.6 eV) for XPS, respectively.

Cyclic voltammetry and chronoamperometry were carried out at room temperature with a CHI 605B electrochemistry workstation in a conventional three-electrode cell. A thin layer of Nafion-impregnated catalyst with a Pd loading of $28 \mu\text{g}\cdot\text{cm}^{-2}$ casted on a glassy carbon rotating disk electrode was used as the working

electrode, with a Pt foil and a saturated calomel electrode (SCE) as the counter electrode and the reference electrode, respectively.

3. Results and discussion

Both the ICP-AES analysis of the average bulk composition and the EDX analysis of a random composition of the Pd–Ni–P/C catalyst approximately give an atomic ratio of 8:1:1 for Pd:Ni:P with a Pd loading of ca. 19.6 wt.% within measurement errors, which suggest a homogeneous compositional distribution throughout the sample. TEM images for Pd–Ni–P/C and Pd–P/C are shown in Fig. 1A and B, spherical metal nanoparticles of both catalysts are uniformly dispersed on carbon black. Particle size and distribution are obtained based on the measurements of 200 non-agglomerated nanoparticles in an arbitrarily chosen area of the TEM images, the average size of the ternary Pd–Ni–P nanoparticles is ca. 4.3 nm, while the average size of Pd–P nanoparticles is 4.2 nm, slightly larger than that of Pd–Ni/C (3.7 nm, i.e., essentially equivalent to that reported in reference 6) as shown in Fig. 1C.

XRD was applied to examine the alloying effects of P and Ni on the Pd lattice. As shown in Fig. 2, the XRD patterns of all the samples are reflective of the fcc crystalline structure with the main Pd (111) peak located at ca. 40°. Nevertheless, the XRD pattern for the as-prepared Pd–Ni/C consists of two additional peaks at 33.5° and 59.2° (marked with asterisks), attributable to Ni(OH)_2 (100) and (110), respectively. Besides, no significant shift of the Pd (111) peak can be seen. These observations indicate a significant presence of unalloyed Ni-phases in the resulting $\text{Pd}_2\text{Ni}_3/\text{C}$, in agreement with those in reference 6. In contrast, the addition of P (as in Pd–P/C) leads to a negative shift of the Pd (111) peak, indicating an expansion of the Pd lattice with the incorporation of P atoms in the interstice of Pd lattice, in agreement to that found for RF-sputtered Pd–P alloy films [15]. Further alloyment with Ni (Pd–Ni–P/C) shifts the characteristic peak positively from that for Pd–P/C. The overall effect makes it slightly smaller than that of Pd/C, revealing a net lattice contraction due to the partial replacement of Pd sites in Pd–P nanoalloy by smaller Ni atoms, in analogy to the shift of XRD patterns for Pd–Ni bimetallic nanoalloys with the increasing addition of Ni [16]. The apparently opposite effects of the alloying elements P and Ni on Pd lattice constant enable conveniently to tune geometric and electronic properties of Pd in the ternary catalyst [17].

XPS was employed to analyze the surface compositions and oxidation states of the components, revealing that the surface

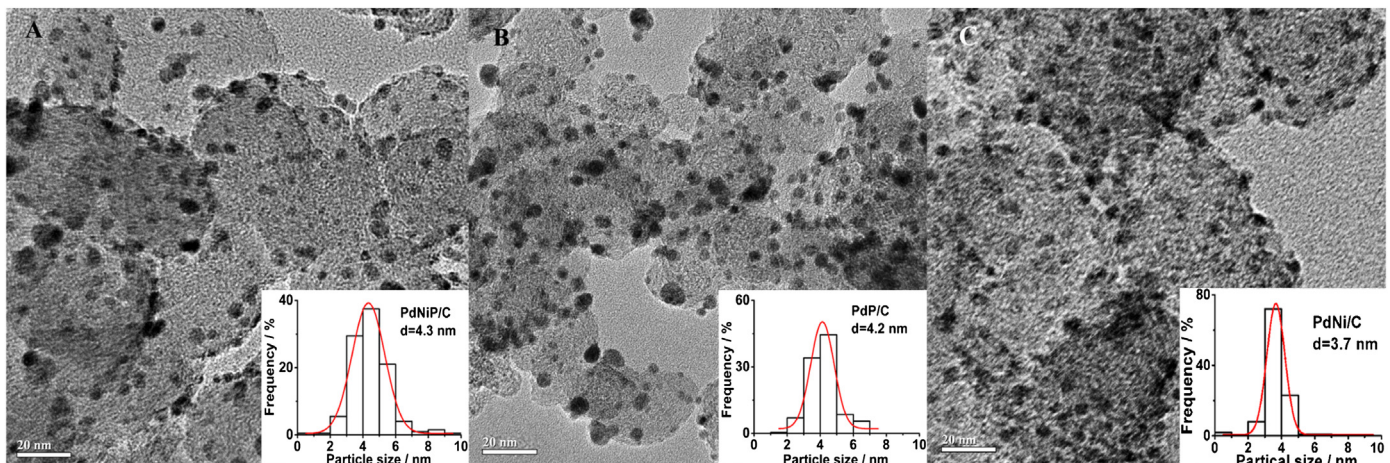


Fig. 1. TEM images and their corresponding particle size distribution histograms: (A) Pd–Ni–P/C, (B) Pd–P/C, (C) Pd–Ni/C catalysts.

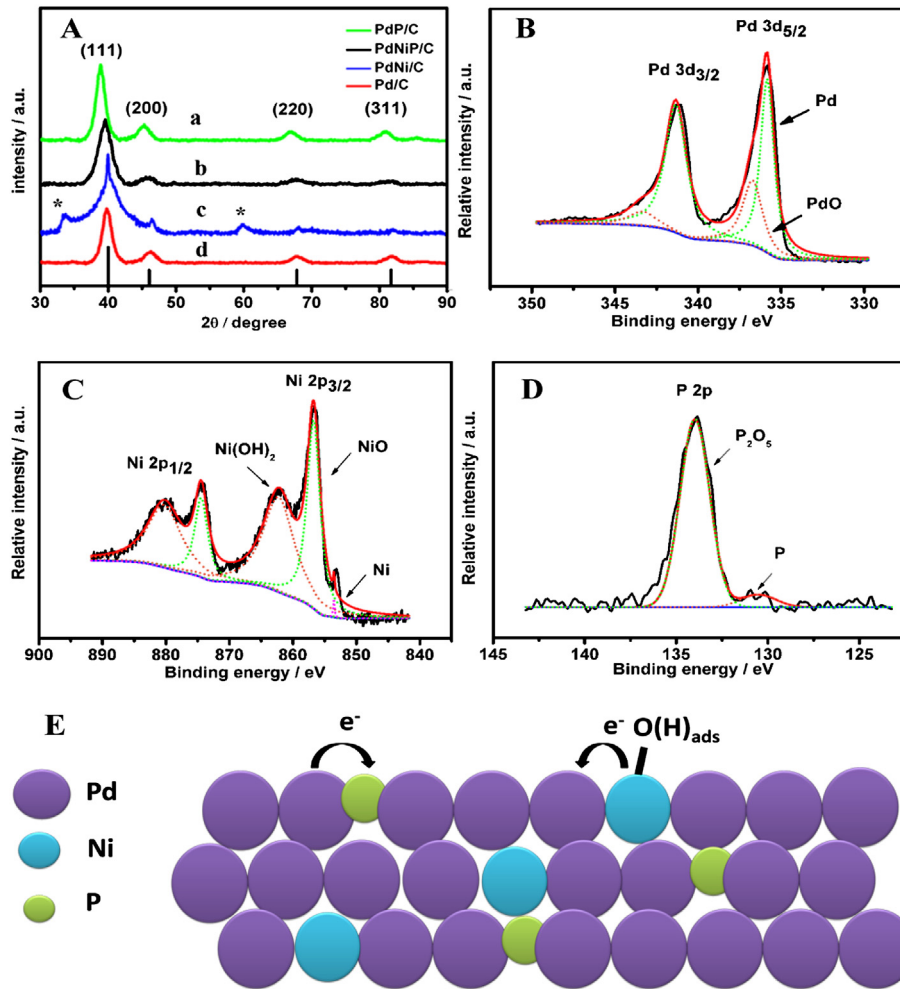


Fig. 2. (A) XRD patterns of the Pd–P/C (curve a), Pd–Ni–P/C (curve b), Pd–Ni/C (curve c) and Pd/C (curve d). The vertical lines correspond to fcc Pd (PDF-#65–6174). (B–D) XPS spectra for Pd 3d (B), Ni 2p (C), P 2p (D) of Pd–Ni–P/C. (E) Scheme of Pd–Ni–P atomic arrangement.

elemental composition is consistent with that determined by ICP-AES, suggestive of insignificant segregation of any specific element at the nanoalloy surfaces. Fig. 2B–D shows the deconvolution of different oxidation states of Pd, Ni and P elements, respectively. The 3d_{3/2} and 3d_{5/2} peaks of Pd in Fig. 2B suggest that Pd(0) species predominates besides minor Pd(II) species on the catalyst surface. The 3d_{3/2} peak of Pd(0) is located at 335.8 eV, shifting positively by 0.7 eV as compared to pure Pd in the literature [18]. In other words, the core-level of Pd shifts down with respect to the Fermi level of Pd, corresponding to a down-shift of the d-band center of Pd due to its alloying with Ni and P. In fact, the consistence of the d-band center shift and the core-level shift of Pt upon alloying with a second metal having a low work function (such as Co or Ru) was well demonstrated by Watanabe et al. using XPS characterization [19]. A suitable downshift of d-band center weakens the adsorption of both reactants and intermediates in a modest manner [20], favoring the electro-oxidation of ethanol. On the other hand, as shown in Fig. 2C, the broad Ni 2p peak may be deconvoluted to five peaks assigned to three different oxidation states. Apart from a few nominally reduced Ni species, Ni is chiefly present in the form of NiO or Ni(OH)₂ at surfaces. The *ex situ* XPS result directs us to reasonably assume that O-containing species readily form on surface Ni sites of the ternary alloy at lower potentials in alkaline media and facilitate the EOR [8], given its essential role in further oxidations of the CO_{ads} to CO₂ (or HCO₃[–]) and

CO₃^{2–} in alkaline media) and the acetaldehyde to acetic acid (or acetate in alkaline media) [4]. For the P 2p narrow spectrum shown in Fig. 2D, a major peak at 134.0 eV and a minor peak at 130.1 eV could be assigned to the oxidized and nominal P species, respectively, as in the case of Pt–Sn–P/C [14]. The binding energy (BE) of nominal P in the ternary nanoalloy shifts negatively by 0.3 eV with respect to that of red phosphorus [14], which may be explained by assuming that P(0) species accepts partial electrons from surrounding metal species [15], as in the case of Pd–P (a shift of –0.3 eV) [21] and Cr–P (a shift of –1.3 eV) [22] alloys. Based on the XRD and XPS results, the Pd, Ni and P arrangement in our ternary catalyst may be depicted in Fig. 2E. The mixed pattern of Ni, P and Pd sites at nanoalloy surfaces lowers the ratio of CO_B to CO_L on Pd sites due to the so-called geometric effect [10,23]. CO_L species adsorb less strongly on Pd sites than CO_B species, which may favor the oxidative removal of the CO_{ads} intermediate.

Fig. 3A shows the cyclic voltammograms (CVs) obtained in 0.5 M NaOH for the Pd/C, Pd–P/C, Pd–Ni/C and Pd–Ni–P/C-covered electrodes with the same Pd loading of 28 $\mu\text{g}\cdot\text{cm}^{-2}$. From the corresponding cathodic peaks around –0.3 V for the reduction of Pd–O(H) species, it may be estimated that the Pd–Ni–P/C, Pd–P/C and Pd/C electrodes expose nearly identical surface Pd sites, and 1.3 times as many as the Pd–Ni/C. The latter may result from the higher content of Ni in the Pd–Ni/C sample [16]. Fig. 3B shows the corresponding CVs in 0.5 M NaOH + 1 M C₂H₅OH for these four

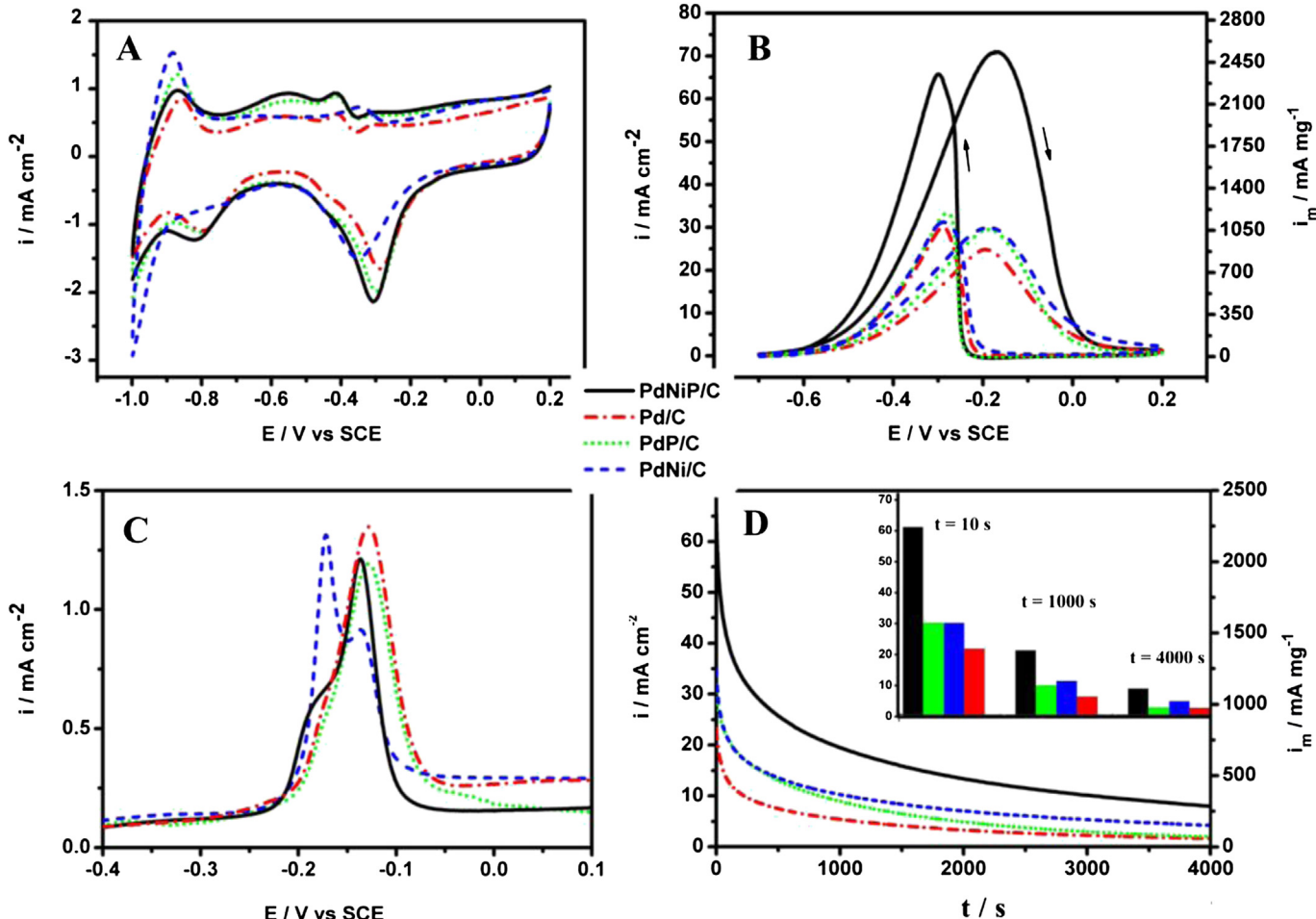


Fig. 3. CVs for Pd-based catalysts in 0.5 M NaOH in the absence (A) and presence (B) of 1 M C₂H₅OH at 50 mV s⁻¹; Anodic stripping curves (C) of CO adlayer at Pd in 0.5 M NaOH at 10 mV s⁻¹; Chronoamperometry (D) on Pd-based catalysts in 0.5 M NaOH + 1 M C₂H₅OH at -0.2 V and 1000 rpm.

catalysts. It can be seen that the Pd–P/C or the Pd–Ni/C shows a mildly enhanced oxidation peak current, and the oxidation peak current on the Pd–Ni–P/C is actually doubled as compared to that on the Pd/C. It may be necessary to point out that when normalized by exposed surface Pd sites the specific oxidation peak current on Pd–Ni/C is higher than that on Pd/C or Pd–P/C and yet significantly lower than that on the Pd–Ni–P/C. The corresponding mass activity of our Pd₈Ni₁P₁/C is 2533 mA·mg⁻¹ Pd, even higher than that of the reported Pd₄₁Ni₃₀Au₂₉/C, i.e., 1403 mA·mg⁻¹ Pd [9]. On the other hand, the onset oxidation potentials on the Pd–Ni–P/C, Pd–Ni/C, Pd–P/C and Pd/C are ca. -0.61, -0.62, -0.56, and -0.55 V, respectively. Intuitively, the negative shift of the onset potential is mainly caused by the addition of Ni rather than P, in agreement with the more oxophilic nature of Ni [8]. Indeed, the anodic stripping potential (Fig. 3C) for a predosed CO monolayer on different catalysts is somewhat similar in trend, following the sequence of Pd/C ≈ Pd–P/C > Pd–Ni–P/C > Pd–Ni/C. Nevertheless, the largest EOR peak current does not necessarily correspond to the most negative shift of the oxidation onset potential.

The long-term activities of these Pd-based catalysts were evaluated with chronoamperometry at -0.2 V in the same electrolyte (Fig. 3D). Again it was found that the Pd–Ni–P/C showed the highest oxidation current density at 4000 s, i.e., 8.0 mA cm⁻², which is 2.0, 3.5 and 4.0 times as high as that observed on the Pd–Ni/C, Pd–P/C and Pd/C, respectively. Based on the above compositional and structural analyses, we may ascribe the outstanding performance of the Pd–Ni–P/C to the suitably weakened adsorption of

surface species on Pd sites [20] and the readily available reactant pair (O-containing species) on neighboring Ni sites [8], thereby to enhance the EOR. Further infrared spectroscopic investigation is under way to clarify which pathway is preferentially enhanced for the EOR on the Pd–Ni–P/C as compared to that on Pd/C.

4. Conclusion

In this work, we synthesize for the first time a Pd–Ni–P/C catalyst targeted for EOR in alkaline media through a facile wet chemical process using sodium hypophosphite as the reducing agent and the source of P. This new catalyst demonstrates a remarkably high catalytic activity and stability for EOR as compared to the state-of-the-art commercial Pd/C, home-made Pd–P/C and Pd–Ni/C catalysts. Structural and electronic characterizations provide evidences to reasonably account for the improved performance of the Pd–Ni–P/C, i.e., the alloyment of Pd with Ni and P imparts catalytic surfaces with appropriate electronic and geometric modifications leading to a modestly weakened adsorption of intermediates on Pd sites, in addition to the oxophilic nature of Ni which is capable of providing the reactant pair OH_{ads} at lower potentials.

Acknowledgments

This work is supported by NSFC (Nos. 21073045 and 21273046) and SMCST (Nos. 11JC140200 and 08DZ2270500).

References

- [1] F. Vigier, S. Rousseau, C. Coutanceau, J.M. Leger, C. Lamy, *Top. Catal.* 40 (2006) 111.
- [2] E. Antolini, E.R. Gonzalez, *J. Power Sources* 195 (2010) 3431.
- [3] C. Bianchini, P.K. Shen, *Chem. Rev.* 109 (2009) 4183.
- [4] Z.Y. Zhou, Q. Wang, J.L. Lin, N. Tian, S.G. Sun, *Electrochim. Acta* 55 (2010) 7995.
- [5] U.B. Demirci, *J. Power Sources* 173 (2007) 11.
- [6] S.Y. Shen, T.S. Zhao, J.B. Xu, Y.S. Li, *J. Power Sources* 195 (2010) 1001.
- [7] E. Antolini, *Energy Environ. Sci.* 2 (2009) 915.
- [8] P.K. Shen, C. Xu, *Electrochem. Commun.* 8 (2006) 184.
- [9] A. Dutta, J. Datta, *J. Phys. Chem. C* 116 (2012) 25677.
- [10] J.Y. Wang, B. Peng, H.N. Xie, W.B. Cai, *Electrochim. Acta* 54 (2009) 1834.
- [11] Y. Okamoto, Y. Nitta, T. Teranishi, S. Teranishi, *J. Chem. Soc. Faraday Trans. 1* (75) (1979) 2027.
- [12] J.Y. Wang, Y.Y. Kang, H. Yang, W.B. Cai, *J. Phys. Chem. C* 113 (2009) 8366.
- [13] L. Zhang, Y. Tang, J. Bao, T. Lu, C. Li, *J. Power Sources* 162 (2006) 177.
- [14] X. Xue, J. Ge, T. Tian, C. Liu, W. Xing, T. Lu, *J. Power Sources* 172 (2007) 560.
- [15] J. Tamaki, S. Nakayama, M. Yamamura, T. Imanaka, *J. Mater. Sci.* 24 (1989) 1582.
- [16] Z.Y. Zhang, L. Xin, K. Sun, W.Z. Li, *Int. J. Hydrogen Energy* 36 (2011) 12686.
- [17] J.R. Kitchin, J.K. Nørskov, M.A. Bartéau, J.G. Chen, *Phys. Rev. Lett.* 93 (2004) 156801.
- [18] J.F. Moulder, W.F. Stickle, P.E. Sobol, K.D. Bomben, in: J. Chastain (Ed.), *Handbook of X-ray Photoelectron Spectroscopy*, Perkin Elmer Corp, Eden Praire, 1992, p. p.181.
- [19] M. Wakisaka, S. Mitsui, Y. Hirose, K. Kawashima, H. Uchida, M. Watanabe, *J. Phys. Chem. B* 110 (2006) 23489.
- [20] L.A. Kibler, A.M. El-Aziz, R. Hoyer, D.M. Kolb, *Angew. Chem. Int. Ed.* 44 (2005) 2080.
- [21] G. Yang, Y. Chen, Y. Zhou, Y. Tang, T. Lu, *Electrochim. Commun.* 12 (2010) 492.
- [22] M. Pelavin, D.N. Hendrickson, J.M. Hollander, W.L. Jolly, *J. Phys. Chem.* 74 (1970) 1116.
- [23] J.Y. Wang, H.X. Zhang, K. Jiang, W.B. Cai, *J. Am. Chem. Soc.* 133 (2011) 14876.